Chemical Engineering Science 117 (2014) 364–375

Contents lists available at ScienceDirect

Chemical Engineering Science

journal homepage: www.elsevier.com/locate/ces

Multi-scale modeling of diffusion and reaction–diffusion phenomena in catalytic porous layers: Comparison with the 1D approach

J.M.C. Pereira, J.E.P. Navalho*, A.C.G. Amador, J.C.F. Pereira

LAETA, IDMEC, Instituto Superior Técnico, Universidade de Lisboa, Mechanical Engineering Department/LASEF, Av. Rovisco Pais, 1, 1049-001 Lisbon, Portugal

HIGHLIGHTS

- A 3D multi-scale bottom-up washcoat model for CO oxidation is herein considered.
- Effective diffusivities are evaluated with the 3D approach and with the random pore model.
- The random pore model results are not satisfactory for all porous structures.
- Reaction–diffusion simulations are performed with the 3D model and with a 1D model.
- Good agreement between both models is observed by considering the 3D diffusivities in the 1D model.

GRAPHICAL ABSTRACT

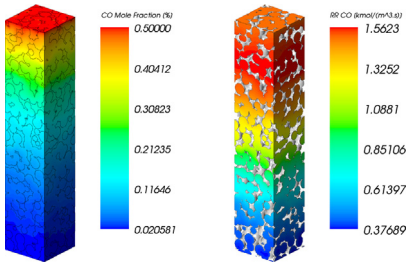

ARTICLE INFO

Article history:
Received 15 April 2014
Accepted 11 June 2014
Available online 23 June 2014

Keywords:
Multi-dimensional reaction–diffusion modeling
Washcoat structure
Diffusional limitations
Digital reconstruction
Catalytic combustion

ABSTRACT

The impact of the catalyst internal structure on the conversion rates of CO oxidation is investigated using a 3D multi-scale bottom-up approach for transport and reaction modeling in isothermal porous catalyst layers. The multi-scale methodology is employed to evaluate effective diffusion coefficients that are further compared with the values predicted with the random pore model. Multi-scale reaction–diffusion simulations are performed and compared with the results of the 1D pseudo-homogeneous, continuum approach.

CO oxidation described by a single-step reaction mechanism is used to demonstrate the methodology, although it is extensible to any set of catalytic reactions. Digital reconstruction techniques are employed to generate porous media with specific structural properties representative of two different length scales (nano and micro). On the nano-scale level, diffusion simulations along the mesopore network are carried out to evaluate effective diffusivity values that are further exported to the micro-scale level where diffusion and reaction–diffusion simulations are considered. Several washcoat layers were reconstructed varying only the grain size distribution and the partial overlapping between micro-particles. Multi-scale diffusion simulations showed that the random pore model is only suitable for specific porous structures. Furthermore, the comparison between the results of the multi-scale and 1D reaction–diffusion models also showed that by providing an accurate estimation of the effective diffusivity data for the 1D model, namely through multi-scale diffusion simulations, instead of the random pore model results, a significant agreement is verified between both models.

* Corresponding author.
E-mail addresses: jose.chaves@tecnico.ulisboa.pt (J.M.C. Pereira), jorge.navalho@tecnico.ulisboa.pt (J.E.P. Navalho), antonio.amador@tecnico.ulisboa.pt (A.C.G. Amador), jcfpereira@tecnico.ulisboa.pt (J.C.F. Pereira).

http://dx.doi.org/10.1016/j.ces.2014.06.028
0009-2509/

1. Introduction

Catalysis is very important in the chemical industry since it is estimated that 90% of the chemical processes developed nowadays involve the use of catalysts in at least one of their steps (Fechete et al., 2012). One of the most widespread applications of catalysis is the automotive exhaust gas after-treatment catalytic converter (Twigg, 2011). Catalysis plays also an important role in the field of energy conversion through hydrogen (Holladay et al., 2009). In this quest for cleaner energy sources and in order to meet the increasingly demanding energetic needs, catalysis may have a key role in improving the processes efficiency (Vlachos and Caratzoulas, 2010) which can be achieved through multi-scale modeling approaches.

In the context of reaction engineering, the typical objective of a multi-scale model is to predict the macroscopic behavior of the reactor from information obtained at the most elementary level (Salciccioli et al., 2011). Therefore, they are usually divided in several physical levels with specific physico-chemical phenomena and a bottom-up (or upscaling) approach is used to progressively pass information from the smallest scale to the largest one (Vlachos et al., 2006). At the most detailed level quantum mechanics is involved and the parameters predicted at this level are used on atomistic simulations that employ techniques such as Molecular Dynamics or Kinetic Monte Carlo Simulations, where transport (e.g. diffusion) and chemistry properties are predicted (Chatterjee and Vlachos, 2007). All these methods are used to obtain unknown parameters that are not easily accessible through experimental data. Finally, at the reactor (macroscopic) scale, simulations with multi-component mass and heat transfer properties are employed. However, coupling the levels of a multi-scale model is still very demanding. Moreover, the wide range of scales and techniques requires a huge effort to be able to understand and control the whole process.

The influence of the washcoat thickness (Hayes et al., 2004), noble metal distribution (Ramanathan et al., 2004) or washcoat shape (More et al., 2006) on the overall performance of catalytic converters used in automobiles has shown that it is important to implement correctly the role of the washcoat structure in the intraphase transport limitations in full-scale models. A similar relevance arises for honeycomb monolith reactors, usually described by single channel models (Irani et al., 2011).

Some studies have incorporated washcoat effects on CFD commercial code predictions, such as reference (Kolaczkowski et al., 2007), that modeled the flow in a catalyst pellet, although the process of diffusion in the catalyst washcoat is not explicitly modeled in the CFD code, but instead with the establishment of a effectiveness factor from an analytical solution for the catalyst. Mladenov et al. (2010) simulated the channel flow of automotive catalytic converters using simple effectiveness factor models and detailed reaction–diffusion models and it was reported that, although the latter are computationally very expensive, they provide the best agreement with the experimental data.

However, these methodologies require a high computational cost and an alternative is to model the porous washcoat separately and evaluate how the species transport and reaction occurs. Examples of this methodology may be found in Keil (1999) where a washcoat was modeled considering a three-dimensional porous medium with multi-component diffusion and it was found that random networks can contribute considerably to the design of optimum porous structures. A model which simulates diffusion, reaction and capillary condensation in a pore network representing a catalyst pellet was developed by Wood and Gladden (2002). The authors calculated the effectiveness factor as a function of pore structure and operating conditions and found that the catalyst effectiveness is very sensitive to the structural properties. Further studies include a methodology to model reaction-transport processes in a digitally reconstructed porous catalyst, with the inclusion of reaction micro-kinetics, which was used for the optimization of the washcoat structure (Kočí et al., 2006).

With the recent developments on multi-scale methodologies, the results obtained by detailed three-dimensional reaction–diffusion models of washcoat layers are exported to larger scales. Kočí et al. (2010) digitally simulate the washcoat formation process at two different scale levels, evaluate the reaction and diffusion of the gas species and export global parameters of the washcoat performance to full-scale monolith channel models. This methodology was further extended to exhaust gas carbon monoxide oxidation in a washcoat layer with an inert part (diffusion barrier) and good agreement was found between the multi-scale model results and experimental data (Novák et al., 2012).

One of the most commonly used methods to determine effective diffusion coefficients is the random pore model (RPM) (Wakao and Smith, 1962), which considers a bimodal pore size distribution as one can find in most of the washcoated catalysts. The parallel pore model (Wheeler, 1955) is also widely used for monodispersed pore systems and generally presents better results. However, in this model a parameter must be estimated (tortuosity), which comes directly from experiments (Satterfield, 1970) hence the better results are reported. Regarding the RPM, Hayes et al. (2000) and Sharma et al. (1991) found an overprediction by 3 to 8 times the experimental value. Furthermore, Beeckman (1991) reported a good match between RPM and experiments. On the other hand Novák et al. (2012) reported a RPM prediction in between one half and one quarter of the experimental data. The different effective diffusivity values reported in the literature can be due to different washcoat structures as a result of different preparation methods (Stutz and Poulikakos, 2008).

The main objective of this research is to use a 3D multi-scale methodology for the virtual prototyping of porous catalyst layers in order to understand the influence of their structural properties on the reaction rates and to compare it with the classical 1D pseudo-homogeneous continuum approach based on empirical correlations for the calculation of effective diffusion coefficients. A multi-scale approach based on the one presented in Novák et al. (2011) is herein considered. Such multi-scale methodology consists in analyzing the structure of the porous catalyst carrier at two different, yet correlated, length scale levels: the nano-scale level and the micro-scale level. The multi-scale analysis used in this work targets the smallest levels of the macroscopic scale of a catalytic converter up to the borders with the mesoscopic scale where the continuum approach can still be considered valid, i.e. the washcoat level. Porous catalytic layers are represented through digitally reconstructed three-dimensional models whose structural properties are then evaluated. CFD simulations with transport and reaction of gas species are then performed in the reconstructed media and finally the influence of the washcoat structure on the overall process is evaluated.

After this introduction the mathematical formulation of the 3D multi-scale and 1D pseudo-homogeneous washcoat models is presented in Sections 2.1 and 2.2, respectively, followed by the numerical models section (Section 2.3). The validation of the multi-scale reaction–diffusion model is thereafter presented in Section 3. In Section 4 the results of multi-scale diffusion simulations for several washcoat layers are presented and compared with the results predicted by the random pore model. Also in this section the performance of the 1D model with two strategies to evaluate the required effective transport data is compared with the results obtained with the 3D multi-scale reaction–diffusion model. The paper ends with summary conclusions (Section 5).

2. Reaction–diffusion models

2.1. 3D multi-scale washcoat model

According to the standards adopted by the International Union of Pure and Applied Chemistry (IUPAC), porous materials can be classified in different kinds depending on their size. Pores with a diameter <2 nm are named micropores, with 2–50 nm are mesopores and with >50 nm are macropores. Following this terminology, the micro- and mesopores are studied in the nano-scale level, while the macropores are studied in the micro-scale level (see Fig. 1).

On the nano-scale level, the formation of the catalyst mesoporous support structure is represented through a cubic shaped medium with a system size of 100^3 nm^3. The system is composed by several primary support nano-particles, with a defined size and shape, that are randomly placed within the medium, although following some correlations. When agglomerated, these particles represent a fraction of bigger micro-particles of the washcoat. From this system several structural and effective transport parameters can be evaluated and then employed on the micro-scale level.

On the micro-scale level a thin section of the whole catalytic layer is considered and therefore its size may vary according to the actual washcoat thickness. The system is composed by catalyst support micro-particles that when agglomerated create macropores among them. Structural parameters are evaluated from the reconstructed layers followed by simulations of diffusion and combined reaction–diffusion. In such simulations, the results obtained at the nano-scale level simulations, in particular effective diffusivities ($D_k^{m,eff}$), are used to describe the species transport rates inside the micro-particles. On this level, overall effective diffusion coefficients ($D_k^{M,eff}$) can be calculated through diffusion-only simulations or averaged reaction rates (R_j^{avg}) can be evaluated through reaction–diffusion simulations and then exported to full-scale models to describe the overall reactor performance (see Fig. 1).

In both scales, the simulations can be carried out using different temperatures and surface species concentrations, so that the whole range of operating conditions of a catalytic reactor may be considered.

2.1.1. Nano-scale mathematical model

In the reconstructed nano-scale medium the transport of species along the pore network is then simulated, taking into consideration that in the catalytic washcoat the transport of gas components occurs only via diffusion. Although this transport occurs at a very small length scale, the continuum approach is still assumed to be valid at this level (Novák et al., 2010). Considering the system to be under steady-state and isothermal conditions the physical phenomena can be represented by the following transport equation:

$$\nabla \cdot (D_{k,K} c \nabla X_k) = 0 \tag{1}$$

where X_k is the local molar fraction of the diffusing gas component k, c is the total mixture concentration and $D_{k,K}$ is the local value of the diffusion coefficient of the component k. At this scale the diffusion occurs predominantly in the Knudsen regime and thus the diffusion coefficient for each species is computed through Eq. (2) that follows:

$$D_{k,K} = \frac{2}{3} r \left(\frac{8RT}{\pi M_k}\right)^{1/2} \tag{2}$$

where $r = r(\mathbf{x})$ is the local pore radius associated with the position $\mathbf{x} = (x, y, z)$, R is the universal gas constant and M_k is the molecular weight of species k.

In order to evaluate the effective diffusivity in the mesoporous medium ($D_k^{m,eff}$), the mass transport is considered to be dominant in one direction (the direction normal to the external washcoat/bulk gas interface – z-direction in this work), which is done by imposing a concentration difference between the two opposite z-boundaries of the nano-scale physical model (pore space of the nano-scale level system – see Fig. 1) and considering a null flux (zero Neumann boundary conditions) across the remaining boundaries. Therefore, the following boundary conditions are imposed to the system:

$$X_k|_{z=0} = X_k^0, \quad X_k|_{z=L} = X_k^1, \quad \left.\frac{\partial X_k}{\partial x}\right|_{x=0,L} = 0, \quad \left.\frac{\partial X_k}{\partial y}\right|_{y=0,L} = 0 \tag{3}$$

where X_k^0 and X_k^1 are the molar fractions imposed on the two opposite boundaries that generate the concentration gradient in the z-direction. From the resultant concentration field the effective diffusion coefficient of the gas component k in the mesoporous structure can be calculated through the equation:

$$D_k^{m,eff} = N_k \frac{L}{c(X_k^1 - X_k^0)} \tag{4}$$

where the term $c(X_k^1 - X_k^0)$ represents the imposed concentration difference of the component k across the medium in the z-direction, L being the size of the reconstructed medium. N_k is the effective Knudsen diffusive molar flux obtained by surface integration

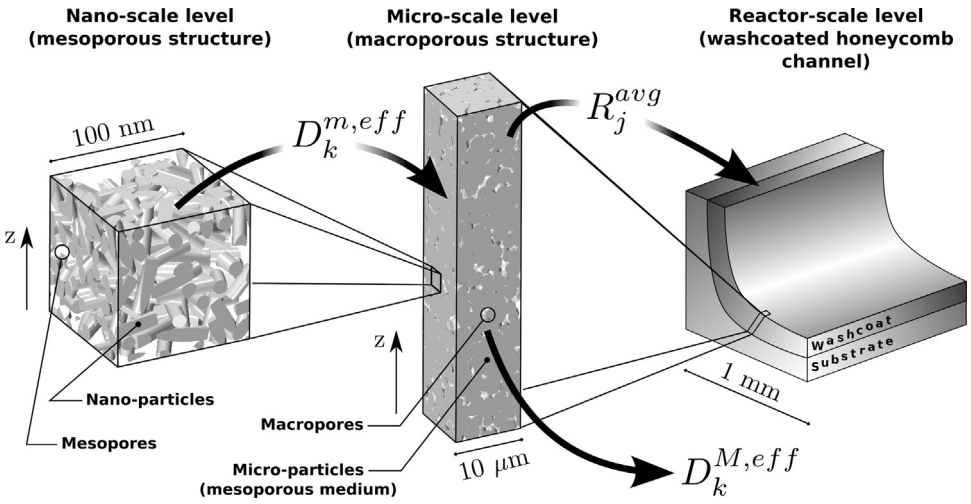

Fig. 1. System decomposition according to the washcoat multi-scale methodology.

of the diffusive flux across an arbitrary cross-section, A_z, perpendicular to the z-direction, chosen in the interval $0 \le z \le L$:

$$N_k = \frac{1}{A_z}\int_{A_z} D_{k,K} c \frac{\partial X_k}{\partial z}\, dx\, dy \tag{5}$$

2.1.2. Micro-scale mathematical model

The micro-scale simulations are performed in order to evaluate the diffusion and combined reaction–diffusion processes inside the washcoat layer. The system is reconstructed with the same techniques used for the nano-scale models and has a typical size of $10 \times 10 \times t$ μm^3 where t is the thickness of the catalytic layer. It consists of a gas phase, representative of the macropores, and a solid phase composed by individual catalyst support micro-particles. Although they are represented as a solid phase, these micro-particles are constituted by clusters of the mesoporous medium considered at the nano-scale level. Therefore, at the micro-scale level, each spatial discretization point of the solid phase includes implicitly the mesopores and, as such, represents an individual system studied by the nano-scale model.

In the generated micro-scale washcoat structure the overall effective diffusivities of gas components inside the layer can be calculated for inert conditions (diffusion-only simulations), analogously to the nano-scale models using Eq. (1). However, at this scale Eq. (1) is solved not only for the gas phase (macropores) but also for the solid phase (mesoporous media), as the latter contains implicitly the mesopores and so the balances for the gas components must be considered there too. As such, the transport of a species k inside the micro-particles is represented through the local diffusion coefficient, D_k, that takes the value of $D_k^{m,eff}$ obtained in Eq. (4). In the macropores, void fraction of the micro-scale model, the species transport is mainly driven by bulk diffusion. Molecular diffusion coefficients for each species are herein computed through the following correlation (Poling et al., 2001):

$$D_{k,b} = \frac{0.00143 T^{1.75}}{P\sqrt{2/(1/M_k + 1/M_{ref})}[(\Sigma_v)_k^{1/3} + (\Sigma_v)_{ref}^{1/3}]^2} \tag{6}$$

where Σ_v is the diffusion volume of each species (see Poling et al., 2001). Applying to the micro-scale species governing equations the same boundary conditions applied to the nano-scale mathematical model, the effective diffusion coefficients along the washcoat layer ($D_k^{M,eff}$) can be analogously calculated through Eqs. (4) and (5).

Reaction–diffusion simulations are performed in order to determine the actual reaction performance observed along the whole washcoat layer. To describe the physico-chemical processes, the following reaction–diffusion equation is applied to all reactive gas phase species considered in reactions $j = 1, \ldots, NR$:

$$\nabla \cdot (D_k c \nabla X_k) + \sum_{j=1}^{NR} (\nu_{k,j} \cdot R_j) = 0 \tag{7}$$

As in the diffusion-only simulations, depending if the solid (porous micro-particles) or the gas phase (macropores) are being considered, the diffusion coefficient (D_k) takes the value computed with Eqs. (4) or (6), respectively. In The second term of the reaction–diffusion equation, $\nu_{k,j}$ represents the stoichiometric coefficient of the gas component k in the reaction j and R_j the respective local reaction rate. The reactions are considered only in the solid phase of the micro-scale level where the catalyst sites are impregnated in the mesoporous support structure. An average concentration of catalytic sites related to the net volume of the mesoporous support particles is considered since the active catalytic sites are not discretized in any physical model considered. The studied washcoat layer is assumed to be at a constant temperature (isothermal conditions).

In this work the total oxidation of CO is considered. A one-step reaction scheme is considered to describe the overall reactants conversion pathway ($CO + 1/2O_2 \rightarrow CO_2$), being its kinetics described by the Langmuir–Hinshelwood rate expression developed by Voltz et al. (1973) for Pt/Al_2O_3 catalysts:

$$R(\mathbf{x}) = \begin{cases} 0 & \text{if } \mathbf{x} \text{ belongs to the gas phase} \\ C^m_{\text{Pt,sites}} \frac{k X_{CO} X_{O_2}}{(1 + K_{inh} X_{CO})^2 T} & \text{if } \mathbf{x} \text{ belongs to the solid phase} \end{cases} \tag{8}$$

where k and K_{inh} are computed through Arrhenius and Van't Hoff equations, Eqs. (9) and (10), respectively. The kinetic parameters considered in Eqs. (9) and (10) are listed in Table 1. $C^m_{Pt,sites}$ is the concentration of catalytic Pt sites related to the net volume of mesoporous alumina.

$$k = k_0 \cdot \exp\left(\frac{-E_a}{RT}\right) \tag{9}$$

$$K_{inh} = K_{inh0} \cdot \exp\left(\frac{E_{inh}}{T}\right) \tag{10}$$

The set of boundary conditions applied to the reaction–diffusion equation (Eq. (7)) is the following:

$$X_k\Big|_{z=t} = X_k^{bnd}, \quad \frac{\partial X_k}{\partial x}\Big|_{x=0,L_x} = 0, \quad \frac{\partial X_k}{\partial y}\Big|_{y=0,L_y} = 0, \quad \frac{\partial X_k}{\partial z}\Big|_{z=0} = 0 \tag{11}$$

where X_k^{bnd} is the boundary value of the components' molar fraction used on the top boundary (the external surface of the washcoat layer) where there is significant mass and heat exchange with the bulk gas flow along the monolith channel. On the remaining boundaries of the micro-scale physical model null species molar fluxes are imposed.

The governing equations are solved numerically and from the results spatially averaged parameters of the 3D system can be evaluated, like the averaged reaction rate and the internal effectiveness factor calculated through Eqs. (12) and (13), respectively, where V_T is the total volume of the studied layer, V_S is the volume of the support micro-particles and R_j^{bnd} is the rate of reaction j at the conditions occurring on the external boundary ($z=t$) of the washcoat.

$$R_j^{avg} = \frac{1}{V_T}\int_{V_T} R_j\, dV \tag{12}$$

$$\eta_j = \frac{1}{V_S \cdot R_j^{bnd}}\int_{V_S} R_j\, dV \tag{13}$$

The averaged reaction rate provides information regarding the amount of reactions that occur in the whole washcoat section. The effectiveness factor quantifies the extent of the diffusional resistances along the porous network by comparing the averaged reaction rate value with the reaction rate observed at the external washcoat surface (where no diffusional limitations are registered). These are important parameters for a full-scale reactor model, as it

Table 1
Kinetic parameters.

Parameter	Value
k_0	2.0×10^{18} K s^{-1}
E_a	90.0×10^3 J mol^{-1}
K_{inh0}	5.0×10^1
E_{inh}	1.0×10^3 K
$C^m_{Pt,sites}$	66.6 mol m^{-3}

is through them that the interaction between reaction and diffusion along the washcoat layer is simultaneously accounted for.

2.2. 1D pseudo-homogeneous washcoat model

The interactions between transport and reaction steps along the washcoat layer have been extensively modeled through 1D continuum models by applying the reaction–diffusion equations or through the application of effectiveness factors computed with the Thiele modulus. The isothermal reaction–diffusion problem in steady-state conditions along the washcoat thickness (z-direction) is described by Eq. (14) where reaction rate values are expressed on a total washcoat volume basis.

$$\frac{\partial}{\partial z}\left(cD_k^{M,eff}\frac{\partial X_k}{\partial z}\right)+\sum_{j=1}^{NR}(\nu_{k,j}\cdot R_j)=0 \tag{14}$$

This equation is applied to all reactive species and is subjected to the same boundary conditions in the z-direction as before the 3D fully distributed micro-scale level model.

The transport coefficients in pseudo-homogeneous washcoat models are described by continuum (effective) values. Several models were proposed in the past for evaluating effective diffusion coefficients based on transport properties of the gas mixture and textural properties of the medium such as porosity and pore size distribution. A widely employed method developed for bidispersed porous systems is the random pore model (Wakao and Smith, 1962) expressed through Eq. (15), where ε^M and ε^m correspond to the macro- and mesoporosities, respectively.

$$D_k^{M,eff}=(\varepsilon^M)^2D_{k,b}+(\varepsilon^m)^2D_{k,K}+\frac{4[\varepsilon^M-(\varepsilon^M)^2]}{1/D_{k,b}+(1-\varepsilon^M)^2/[(\varepsilon^m)^2D_{k,K}]} \tag{15}$$

The random pore model was proposed for porous materials prepared by compressing (micro/meso) porous powders. The method accounts for three parallel diffusion paths, namely diffusion in micro/mesopores, in macropores and in a series of micro/mesopores and macropores, properly considered through the first, second and third terms of the right hand side of Eq. (15).

In this work, bulk and Knudsen regimes of diffusion were neglected in Eq. (15) at the micro- and macro-pores, respectively, as they were in the multi-scale model formulation due to their minor importance. The evaluation of effective diffusion coefficients through Eq. (15) requires only the following structural parameters: mesoporosity, mean mesopore radius and macroporosity. It is worth noting that the mesoporosity considered in the random pore model is expressed on a total washcoat volume.

Once a converged numerical solution of Eq. (14) is found the effectiveness factor can be calculated through Eq. (16).

$$\eta_j=\frac{1}{tR_j^{bnd}}\int_t R_j\,dz \tag{16}$$

2.3. Numerical models

The commercial package Star-CCM+ version 6, a CD-Adapco product, was used for the numerical solution of the 3D multi-scale washcoat model, including the CAD modeling and mesh generation, as it is a commercial CFD code that has been tested and verified against several validated benchmark engineering problems, and is therefore suitable to the task.

The species mass balance equations were solved with a segregated species model. This model solves, for a mixture of kk components, $kk-1$ transport equations sequentially. The mass fraction of the last declared species (a diluting species) is evaluated in order to respect mass conservation.

The fluid was modeled as an ideal multi-component gas at steady-state and isothermal conditions. The addition of the reactions (in reaction–diffusion simulations) was modeled through a premixed reacting flow system, homogeneous reactor, using the operator splitting algorithm for the chemistry model and a user-defined reaction rate model.

Regarding the 1D pseudo-homogeneous washcoat model an in-house version of the PREMIX code (Kee et al., 1985) was developed to solve the mathematical model. The governing equations were numerically implemented as a systems of non-linear algebraic equations through finite difference approximations. The numerical solution was achieved through the application of the PREMIX native solver (TWOPNT) that is based on a damped Newton method. A uniform mesh with enough grid points to guarantee a converged mesh-independent numerical solution was considered.

3. Multi-scale model validation

In order to make the validation of the multi-scale model, the overall methodology is demonstrated on the example of CO oxidation in a $Pt/\gamma-Al_2O_3$ washcoat layer and the results are compared with those reported in Novák et al. (2011) for similar conditions. The procedure includes the generation of the porous support and the solution of the diffusion and reaction–diffusion equations in the final virtual washcoat layer in order to obtain volume-averaged parameters. Novák et al. (2011) carried out the reconstruction of the porous structures with a method based on virtual packing of particles with a defined shape and size, followed by partial sintering and the resulting porous medium is represented by a discrete phase function containing information about the volume fraction of each phase in each voxel: solid phase or gas phase. In this work, instead, the superposed spheres method (dos Santos et al., 2002) is employed, where an exclusion factor (F_E) is used to control the partial overlapping among particles.

3.1. Nano-scale simulation

To reproduce the nano-scale simulation, a mesoporous medium was reconstructed with the superposed spheres method using cylinder-shaped particles and following the input parameters listed in Table 2. The resulting structure is represented in Fig. 2, both the solid part and the respective pore space (computational domain). The pore size distribution is then evaluated and shown in Fig. 3, where the resulting distribution is compared with the reference data (see Novák et al., 2011). It can be seen that both distributions are very similar and, as such, the reconstructed medium can be assumed sufficiently similar to the reference structure.

After generating the structure, the effective diffusivity of CO through the mesopores was evaluated, imposing a concentration difference between the top and down z-boundaries. Novák et al. (2011) made an equidistant spatial discretization of the domain (in both solid and porous phases), with a discretization step of 1 nm,

Table 2
Properties of the reconstructed mesoporous structure.

Structural parameter	Value
Cylinder length (l_c^m)	20 nm
Cylinder diameter (d_c^m)	10 nm
Porosity (ε^m)	0.43
Exclusion factor (F_E)	0.0
System size (L^3)	100^3 nm^3

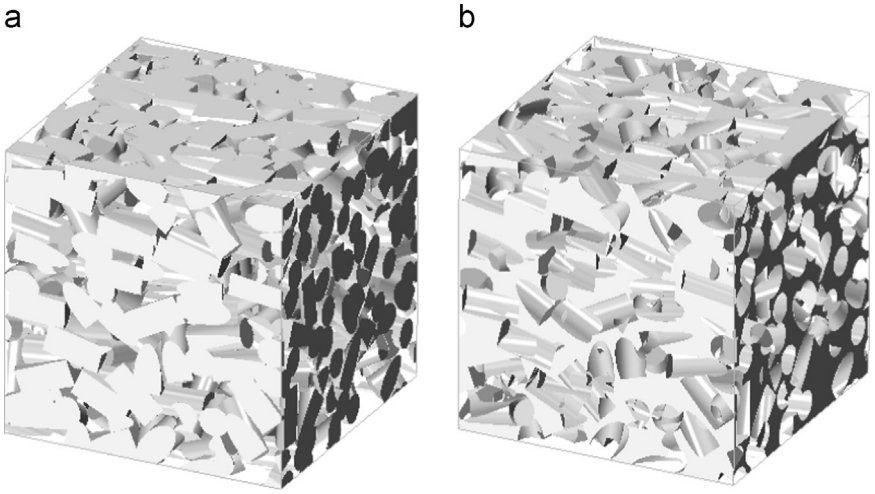

Fig. 2. Generated mesoporous structure: (a) reconstructed mesoporous support, (b) corresponding pore space.

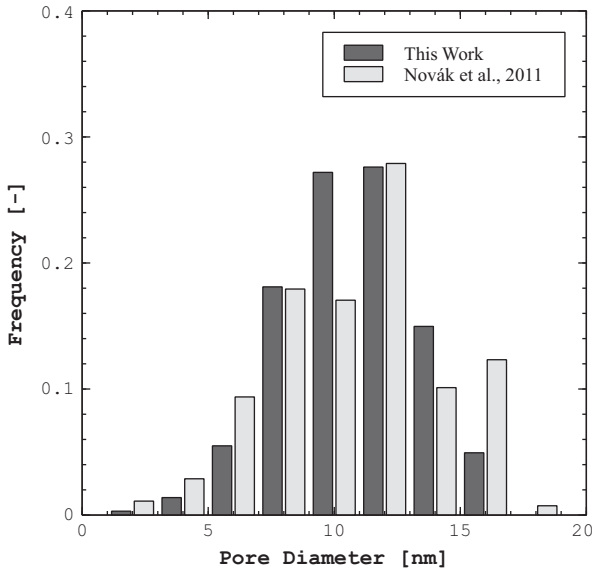

Fig. 3. Pore size distributions of the mesoporous medium generated in this work and the structure reported in Novák et al. (2011).

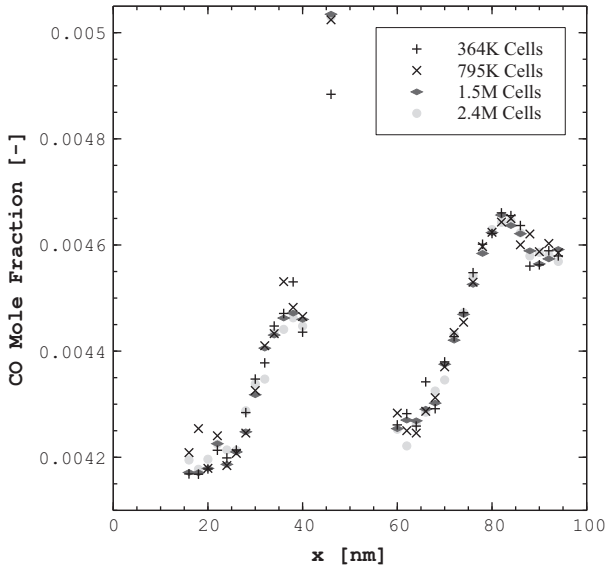

Fig. 4. Mesh convergence on the CO mole fraction profile along the *x*-axis of the mesoporous medium (T=298.15 K).

and solved the resulting transport equation considering the diffusion term null in the voxels belonging to the solid space. In this work, however, only the porous space of the reconstructed medium is modeled (Fig. 2b), as there is no gas flow inside the solid cylinders. As such, a wall boundary is considered between the pore–solid interface and the diffusion equation is only solved for the pore phase.

Taking into consideration that the numerical solution is dependent on the size of the mesh, a convergence analysis with mesh refinement was performed in order to check if the solution was converged. The convergence study was performed using the CO mole fraction profile obtained from a line probe that intersects the middle of the structure along the *x*-axis. The results obtained with four different polyhedral meshes are presented in Fig. 4. Assuming that the most refined model (with 2.4 million cells) is the closest to the right solution, the mesh with 1.5 million cells shows a good fitting in the concentration profiles. Furthermore, this mesh is already refined enough to be able to catch some geometrical details like sharper corners and edges and is therefore the mesh used for the simulations.

Eq. (1) was solved for the domain considering the Knudsen diffusion regime at a constant temperature of 298.15 K. From the converged concentration field the diffusive molar flux of CO through the medium was calculated, as well as the respective effective diffusivity (Eq. (4)). The calculated CO effective diffusion coefficient in the mesoporous medium corresponds to 3.6×10^{-7} m^2/s and approximates very well the value obtained in Novák et al. (2011) with a relative error inferior to 8%. This difference can be due to the slight shift to smaller pore diameters of the generated mesoporous structure in comparison with the reference structure, as reported in Fig. 3, which leads to smaller Knudsen diffusion coefficients and consequently to a slower diffusion regime through the pore network. Nonetheless, the obtained results for the nano-scale level are well approximated and therefore the model can be considered validated at this scale.

3.2. Micro-scale simulation

For the micro-scale physical model the reconstruction technique employed before for the nano-scale structure was used but with spheres as primary particles according to the specifications listed in Table 3. The system corresponds to a slice of the monolith washcoat, being the thickness of the layer equal to 50 μm. The pore size distribution of the macroporous medium was evaluated

Table 3
Properties of the reconstructed macroporous structure.

Structural parameter	Value
Sphere diameter (d_s^M)	2.4 μm
Porosity (ε^M)	0.25
Exclusion factor (F_E)	0.7
System size ($L_x \times L_y \times t$)	$10 \times 10 \times 50\ \mu m^3$

Table 4
CO effective diffusion coefficients in the mesoporous ($D_{CO}^{m,eff}$) and macroporous ($D_{CO}^{M,eff}$) media at 298.15 K.

	$D_{CO}^{m,eff}$	$D_{CO}^{M,eff}$
This work	3.6×10^{-7} m^2/s	2.8×10^{-6} m^2/s
Novák et al. (2011)	3.9×10^{-7} m^2/s	3.0×10^{-6} m^2/s
Relative error	0.077	0.067

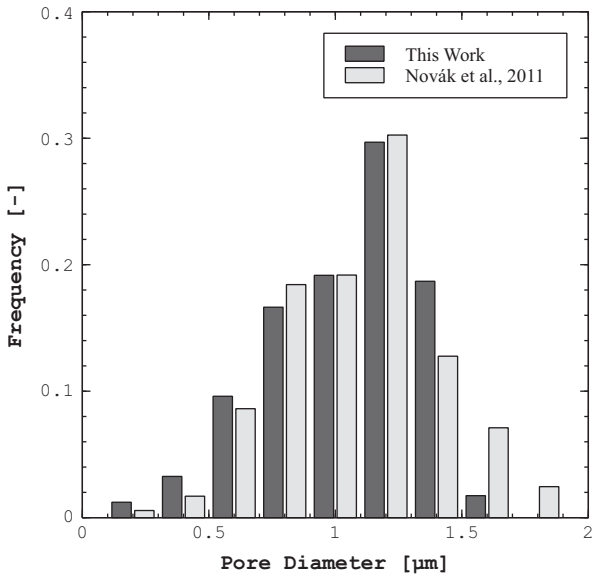

Fig. 5. Pore size distributions of the macroporous medium generated in this work and the structure reported in Novák et al. (2011).

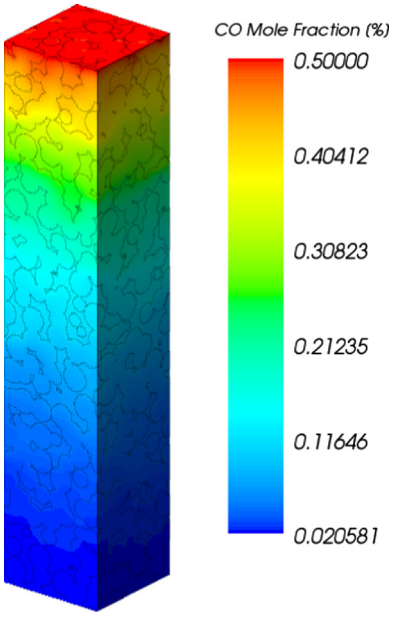

Fig. 6. CO molar fraction field plotted on the boundaries of the macroporous system. Operating condition: $T = 503.15$ K and $X_{CO}^{bnd}/X_{O_2}^{bnd}/X_{N_2}^{bnd} = 0.50\%/2.0\%/\ 97.5\%$.

and compared with the one obtained Novák et al. (2011). Fig. 5 shows that both distributions are very alike, with small differences between the two media due to the use of different reconstruction techniques.

After reconstructing and evaluating the pore size distribution of the macroporous medium, the effective diffusivity through the medium was evaluated in order to validate the overall methodology under non-reacting conditions. The procedure applied was analogous to that applied for the nano-scale level, where a concentration difference between the two opposite z-boundaries was imposed. In the macro-scale level despite existing solid and porous phases the gas flows in both of them because the solid phase implicitly includes mesopores. Therefore, all the medium is discretized and the two different phases are differentiated by the diffusion coefficient: in the solid phase it equals the effective diffusivity, $D_k^{m,eff}$, previously calculated in the nano-scale simulation, and in the gas phase it corresponds to the molecular diffusion coefficient evaluated with Eq. (6). As by Novák et al. (2011), the medium was uniformly spatially discretized through a trimmed mesh with the size of 0.1 μm, leading to a mesh of 5.0 million cells.

After obtaining a converged concentration field, the diffusive molar flux of CO across an arbitrary section perpendicular to the z-direction is calculated, leading to the overall effective diffusivity ($D_{CO}^{M,eff}$) of the medium shown in Table 4. A good agreement is observed between the current results and those reported in Novák et al. (2011) even though the obtained values are slightly smaller than the reference values. This evidence can be explained by the fact that the effective CO diffusion coefficient calculated in the nano-scale simulation level ($D_{CO}^{m,eff}$), used for the mesoporous phase of the macroporous structure, is smaller than the value reported in Novák et al. (2011), which leads to a slower diffusion rate in the mesopore network and consequently to a lower overall effective diffusivity. Nonetheless, the generation of a porous medium with specific properties and the overall methodology under non-reactive conditions (inert washcoat layer) can be said to be validated.

After the characterization of the porous structure, the reaction–diffusion simulations can be performed. An example of the reaction–diffusion simulation results obtained at this level is shown in Figs. 6 and 7, for a temperature of 503.15 K and boundary concentrations on the external surface of $X_{CO}^{bnd} = 0.5\%$, $X_{O_2}^{bnd} = 2.0\%$ and $X_{N_2}^{bnd} = 97.5\%$. The obtained profiles are similar to those presented by Novák et al. (2011) for the same conditions.

The spatially averaged effectiveness factor can then be evaluated (Eq. (13)), as well as its dependence on the surface species concentration and temperature, which is presented in Fig. 8a. A good agreement is observed between the current effectiveness factor results and the reference values reported in Fig. 8b.

At low temperatures a complete absence of mass transport limitations along the porous layer is observed by the value of the effectiveness factor ($\eta = 1$). This is justified by lower reaction rate values comparing to the rates of species diffusion along the washcoat layer. However, increasing the temperature the effectiveness factor decreases denouncing an increase in the species diffusion resistances and consequently a decrease more or less pronounced of the reaction rate value along the washcoat layer as Fig. 7 shows.

A general good agreement is found between the results evaluated with the current methodology and the reference results for the nano- and micro-scale levels, under non-reactive and reactive conditions. Slight deviations are believed to be caused essentially by employing different media reconstructions strategies.

4. Results and discussion

Several washcoat layers were generated to evaluate the effective diffusion rates and compare them to the predictions carried out with the application of the random pore model. The micro-particles of all digitally reconstructed washcoat samples are composed by the mesoporous structure considered in Section 3.1 with a mesoporosity on a total washcoat volume equal to 32.25% ($=\varepsilon^m-\varepsilon^m\varepsilon^M$). The macroporous media generation follows the parameters listed in Table 5 considering a constant macroporosity ($\varepsilon^M=0.25$) for all samples.

Fig. 9 presents the cumulative pore size distribution function for each macroporous structure. The pore size range for each macroporous structure is within the typical range reported in the literature for Al_2O_3 washcoats (Hayes et al., 2000; Kočí et al., 2010; Salejova et al., 2011). In Fig. 9 it can also be observed that by increasing the grain size with a constant exclusion factor, the pore size distribution shifts to larger pore sizes and slightly widens the pore diameter range. A shift to lower pore sizes is also noticeable by increasing the overlapping between micro-particles or adding to the macroporous medium smaller micro-particles in a specific proportion.

In the reconstructed media the overall effective diffusivity of CO in a bath mixture of O_2, CO_2 and N_2 at atmospheric pressure was evaluated through the multi-scale methodology, considering inert washcoat layers with an imposed concentration difference and for different temperatures. The obtained results are presented in Fig. 10, where it is also shown the effective diffusivity curve computed through the random pore model.

For each porous structure the effective diffusion coefficient of CO increases by increasing the temperature due to a relative increase of the molecular diffusion rate in relation to the Knudsen diffusion rate with temperature ($D_{CO,b}/D_{CO,K}\propto T^{1.25}$ see Eqs. (2) and (6)). For each temperature the different effective diffusion coefficient values observed for each medium are essentially justified on the basis of different macropore tortuosities. Following this criterion, the structures S4 and S5 have a pore network with the lowest and highest tortuous path, respectively. It is worth noting that the different transport rates observed for each medium at each temperature are not an outcome of different macroporosities (macroporosity is kept constant for all structures) neither a consequence of the macropore size distribution because the Knudsen regime of diffusion (dependent on the pore size) was neglected in the macropore diffusion calculations.

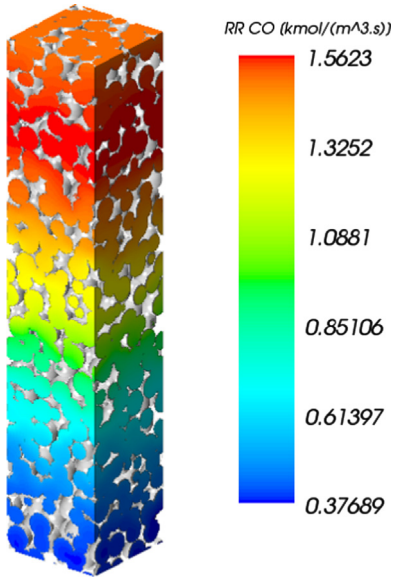

Fig. 7. Reaction rate values plotted on the boundaries of the macroporous system. Operating condition: $T=503.15$ K and $X^{bnd}_{CO}/X^{bnd}_{O_2}/X^{bnd}_{N_2}=0.50\%/2.0\%/97.5\%$.

Table 5
Properties of the reconstructed macroporous media ($\varepsilon^M=0.25$).

Macroporous structure	$d^M_{s,1}$ [μm]	$d^M_{s,2}$ [μm]	$d^M_{s,3}$ [μm]	Mixing ratio	F_E
S1	–	–	1.2	–	0.0
S2	–	–	1.2	–	0.5
S3	–	2.4	–	–	0.0
S4	–	2.4	–	–	0.7
S5	5.0	–	–	–	0.0
S6	5.0	–	–	–	0.5
S7	5.0	–	1.2	1:16	0.0
S8	5.0	–	1.2	1:16	0.5
S9	5.0	2.4	–	1:8	0.0
S10	5.0	2.4	–	1:8	0.5
S11	5.0	2.4	1.2	1:4:16	0.5

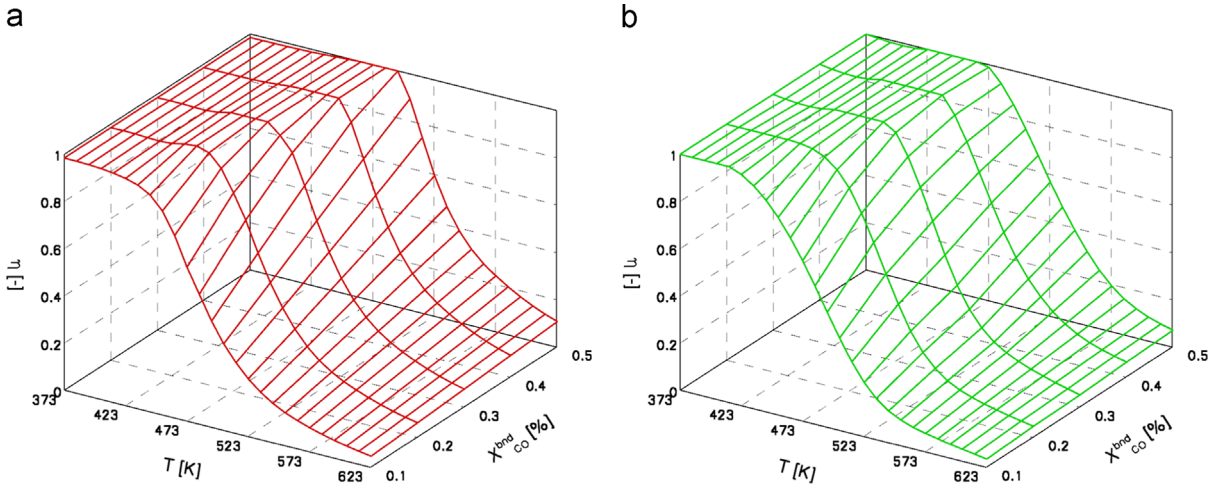

Fig. 8. Spatially averaged effectiveness factor (η) with dependence on CO surface concentration and temperature: (a) this work, (b) Novák et al. (2011).

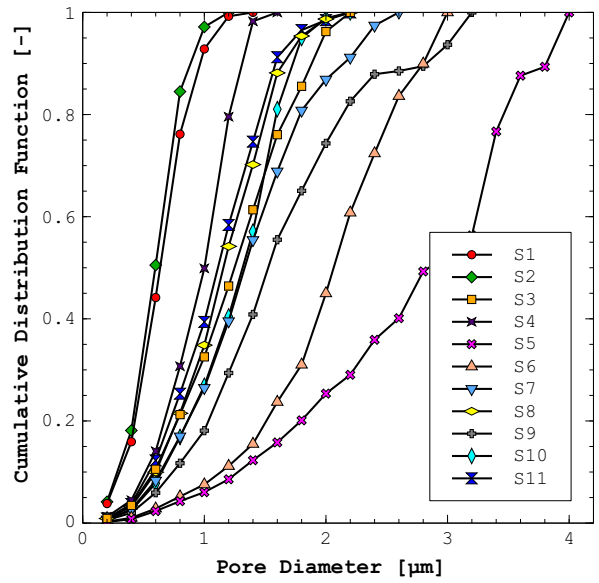

Fig. 9. Cumulative pore size distribution function for each macroporous medium.

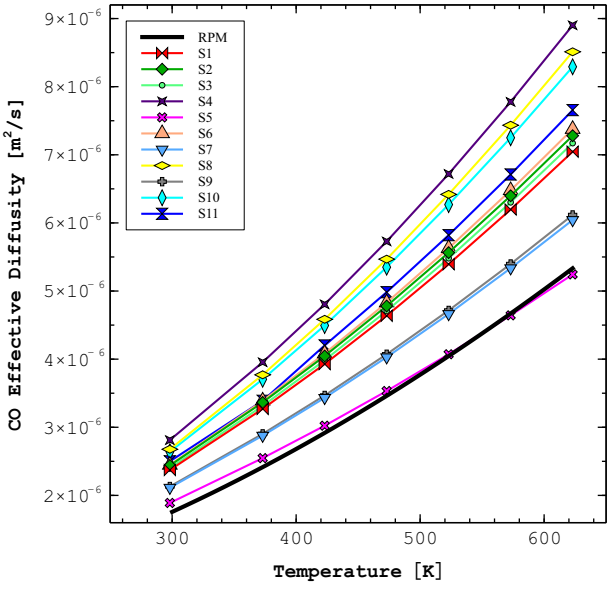

Fig. 10. CO effective diffusivities calculated through the multi-scale methodology (for each medium) and through the random pore model.

A large range of CO effective diffusion coefficients are registered for the porous layers considered at each temperature. Along the temperature range considered in Fig. 10 the random pore model only predicts acceptable values for the porous structure S5 which is the structure that provides the lowest mass transport rates. The effective diffusivity in the remaining samples is higher than that predicted by the random pore model. In particular, for the structure S4 and in the range of temperatures considered the random pore model underestimates the effective diffusion coefficients of CO by about 37–74%. The large range for the transport data supports the finding that physical parameters related with the macroporous structure other than those considered in the random pore model may exert an important role in the actual effective diffusion coefficients.

The impact of different macroporous structures is further evaluated in reaction–diffusion simulations. The 1D pseudo-homogeneous reaction–diffusion mathematical model (described in Section 2.2) is employed considering the effective diffusivities evaluated through the random pore model and the results are compared with those obtained through the application of the multi-scale reaction–diffusion methodology. In this study, the porous structures S2, S4 and S7 were chosen for multi-scale simulations. Typical dependencies on surface operating conditions of the effectiveness factor and spatially averaged reaction rate computed with the 1D and multi-scale models for the three washcoat structures are shown in Fig. 11a and b, respectively.

Analyzing the results, it is possible to see that the global trends of the effectiveness factor and averaged reaction rate are the same for both models (1D and 3D multi-scale reaction–diffusion models) and independent of the macroporous structure considered. At low system temperatures a regime of operation without diffusional limitations is observed by effectiveness factors near 1.0. However, increasing the temperature the relative rate of species consumption/production increases in relation to the rate of species transport by diffusion along the washcoat layer and as a result, increased species concentration gradients will be noted and concluded by a low effectiveness factor value. Even though a remarkable decrease on the effectiveness factor and ultimately on catalyst utilization becomes noticeable by increasing the temperature, the washcoat application at high operating temperatures is still largely profitable because an increase in the averaged reaction rate is continuously observed.

The multi-scale model results for the three porous structures (MS-S2, MS-S4 and MS-S7) presented in Fig. 11a and b show that higher effectiveness factors and averaged reaction rate values are attained for structures that allow higher mass transport rates along the pore network. The 1D reaction–diffusion model with effective diffusion coefficients computed through the random pore model (1D-RPM) underpredicts the averaged reaction rate values for the three structures in a similar manner to the previous one observed for the CO effective diffusion coefficients evaluated through the random pore model and through the multi-scale diffusion simulations (see Fig. 10). For the structures S7, S2 and S4 the difference between the transport coefficients evaluated through the random pore model and the multi-scale model is well correlated with the difference between the 1D and the multi-scale reaction–diffusion models for such structures. The performance of the 1D model coupled with the random pore model becomes more unsuitable for the structure S4 than for the structure S7.

Fig. 12a and b present the averaged mole fraction profiles of CO and CO_2 in cross-sections along the washcoat thickness calculated through the multi-scale (MS) and the 1D reaction–diffusion models for the structures S4 and S7 considering two operating conditions. Concerning the 1D model, two strategies to evaluate the required effective diffusion coefficients were employed: the random pore model (1D-RPM) and the multi-scale diffusion simulations for each structure (1D-MS). Table 6 lists the effectiveness factors computed through the modeling procedures described above for the structures S4 and S7 regarding the operating conditions considered in Fig. 12a and b.

The comparison of the mole fraction profiles obtained with the multi-scale model for each structure, between the two operating conditions, allows us to reinforce that increasing the layer temperature and reactive species composition, higher reaction rates will be observed and the reaction kinetics will be no longer equilibrated by the underlying transport mechanisms. As a consequence, higher transport limitations will be expected (sharper profiles near the external boundary – located at $z = 50\ \mu m$) and lower effectiveness factors will be observed as Table 6 reports.

For both operating conditions the multi-scale model results show steeper species mole fraction profiles for the structure S7 than for the structure S4, which is in full agreement with the lower rates of species diffusion observed for the structure S7 compared

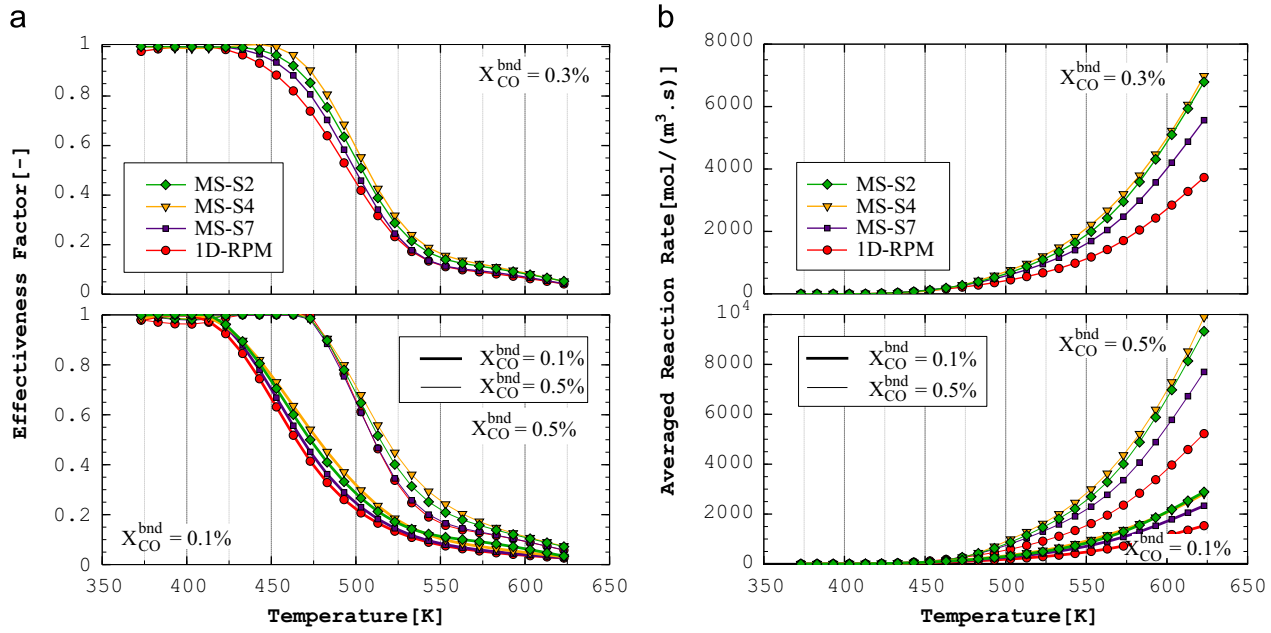

Fig. 11. Effectiveness factor (a) and spatially averaged reaction rate (b) computed with the 1D pseudo-homogeneous (1D-RPM) and multi-scale (MS) reaction–diffusion models for the structures S2, S4 and S7 considering three surface mixture compositions ($X_{CO} = X_{CO_2} = \{0.1; 0.3; 0.5\}\%, X_{O_2} = 2.0\%$ and N_2 to balance) over the temperature range 373.0–623.0 K.

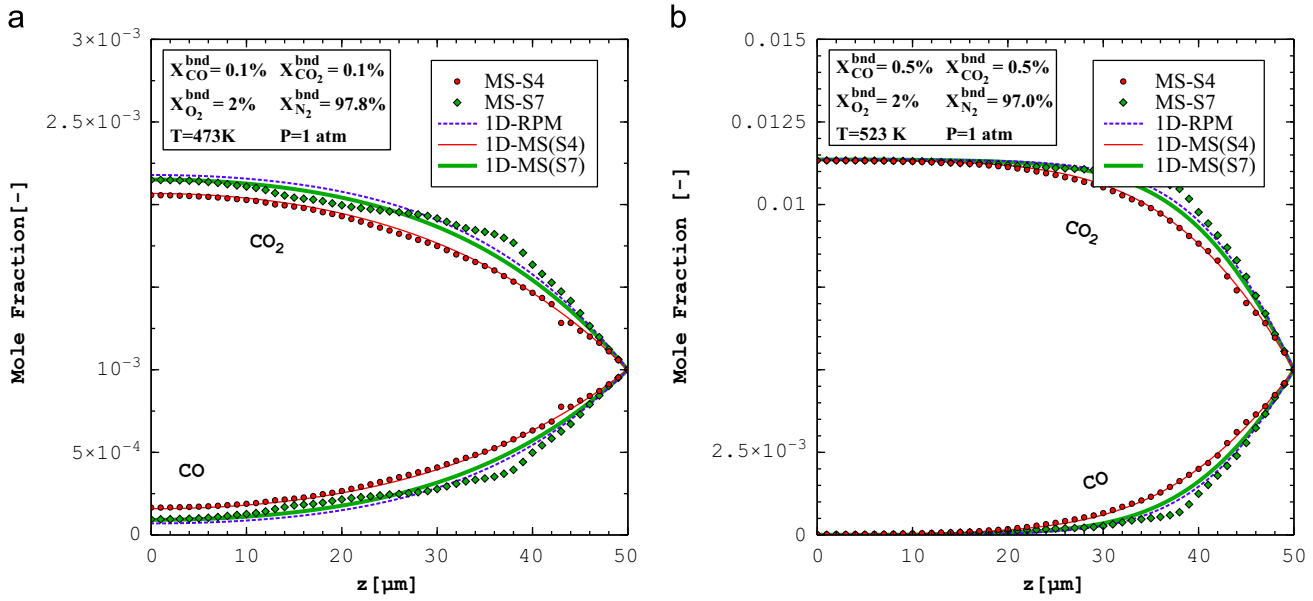

Fig. 12. Averaged mole fraction profiles of CO and CO_2 along the washcoat thickness evaluated with the multi-scale methodology (MS) for the structures S4 and S7 and with the 1D reaction–diffusion model considering effective diffusivities computed with the RPM (1D-RPM) and with multi-scale diffusion simulations for the structure S4 and S7 (1D-MS(S4) and 1D-MS(S7)): (a) $T = 473$ K and $X_{CO}^{bnd}/X_{O_2}^{bnd}/X_{CO_2}^{bnd}/X_{N_2}^{bnd} = 0.10\%/2.0\%/0.10\%/97.8\%$, (b) $T = 523$ K and $X_{CO}^{bnd}/X_{O_2}^{bnd}/X_{CO_2}^{bnd}/X_{N_2}^{bnd} = 0.50\%/2.0\%/0.50\%/97.0\%$.

Table 6
Effectiveness factors evaluated with the multi-scale and 1D reaction–diffusion models. Operating conditions of Fig. 12.

	Op. conditions	MS		1D		
		S4 (%)	**S7** (%)	**RPM** (%)	**MS(S4)** (%)	**MS(S7)** (%)
η	Fig. 12a	54.08	45.17	41.42	52.71	44.63
	Fig. 12b	45.26	35.38	33.74	43.77	36.29

with the rates of diffusion along the structure S4 (see Fig. 10). Consequently, the CO oxidation reaction carried out along the medium S4 attains higher effectiveness factors than the same reaction with equal external conditions along the structure S7 as Table 6 supports. Therefore, the structure S4 allows us to achieve a higher CO absolute conversion than the structure S7.

The profiles evaluated with the multi-scale model show an irregular behavior comparing with the 1D model results due to the model formulation: the multi-scale model takes into account the 3D distribution of the pore space whereas the 1D model considers textural and transport data as continuum (effective) values. The multi-scale profiles of the structure S7 are more irregular than the multi-scale profiles of the medium S4 which can be justified on the basis of the pore size distribution of both structures: the pore size range of the structure S7 is larger than that of the structure S4 (see Fig. 9).

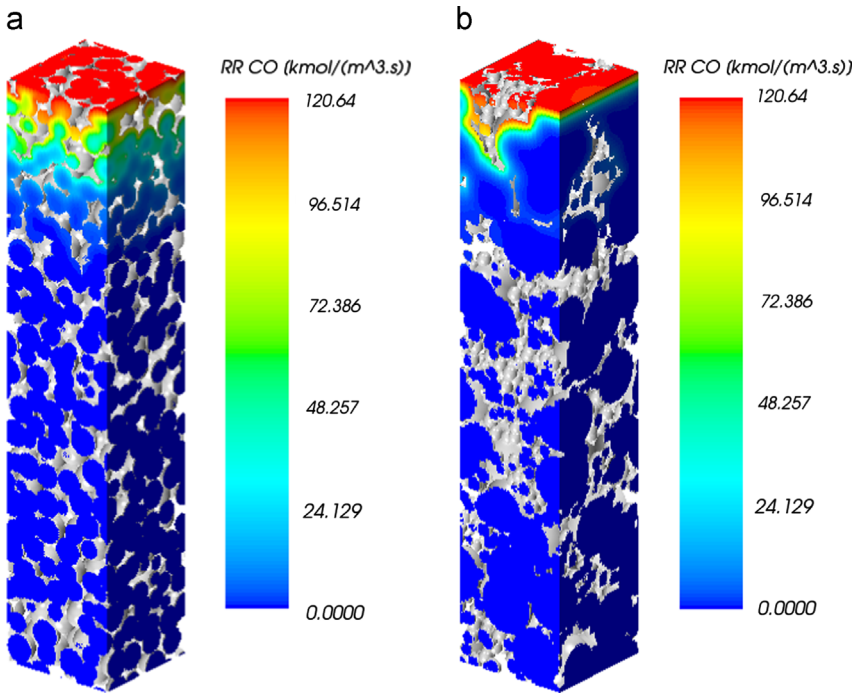

Fig. 13. Reaction rate values plotted on the boundaries of two macroporous structures: (a) structure S4, (b) structure S7. Operating condition: $T = 623$ K and $X_{CO}^{bnd}/X_{O_2}^{bnd}/X_{CO_2}^{bnd}/X_{N_2}^{bnd} = 0.50\%/2.0\%/0.50\%/97.0\%$.

Fig. 12a and b also reveal that the 1D model results computed with effective transport coefficients imported from multi-scale diffusion simulations agree fairly well with the results of the multi-scale reaction–diffusion model. On the other hand, the 1D reaction–diffusion model coupled with the random pore model shows poor results. Table 6 sustains such evidences in terms of effectiveness factors. These conclusions suggest that with an accurate estimation of the transport data for each medium (imported from multi-scale diffusion simulations) the performance of the 1D model tends to approach the behavior exhibited by the multi-scale model. This is an important remark for full-scale reactor modeling efforts where intraporous diffusional limitations are still under interest and are considered through coupling strategies between a washcoat model and a full-scale reactor model. In fact, instead of pre-computing averaged reaction rate values over a plausible range of operating conditions and then interpolating such data and importing it for a full-scale reactor model, the full-scale reactor model can be directly coupled with a 1D washcoat model that employs effective transport coefficients evaluated for a specific porous structure through the multi-scale diffusion model. This strategy would bring significant advantages in terms of computational time over the interpolation approach (explored for instance in Kočí et al., 2010 and Novák et al., 2011) for a kinetic scheme that depends on several local mixture parameters (temperature and several species composition) since it would become unpractical the pre-computation of a large data set to cover all possible combinations among parameters that play a kinetic role.

Considering external conditions that lead to very high reaction rates, the transport limitations increase and a dramatic scenario is approached where only the outermost catalyst surfaces of the entire washcoat layer are available for reaction. This scenario can be observed in Fig. 13a and b for the structures S4 and S7, respectively. For both porous structures the majority of the washcoat layer becomes inaccessible to reactive species. As a consequence, low effectiveness factor values are expected in such conditions (7.78% and 8.51% for the structures S4 and S7, respectively). These extreme cases denounce the need to determine the extent of transport limitations in order to evaluate the amount of catalyst required for specific reaction conditions.

5. Conclusions

A 3D fully distributed mathematical model for transport and reaction in catalyst layers was presented and applied to porous supports that were digitally reconstructed on two different levels: nano and micro. A commercial CFD code was employed to simulate the processes of diffusion and reaction–diffusion in the generated porous structures considering a multi-scale approach to transfer the species transport rates from the nano- to the micro-scale level. The methodology was successfully validated against reference data for reactive and non-reactive conditions.

Several washcoat layers were reconstructed considering for all of them the same mesoporous system (nano-scale geometry) and the same macroporosity but varying the grain size distribution and the overlapping between support micro-particles. The Multi-scale CO diffusion simulation results for such structures showed that a large range of effective diffusion coefficients are obtained for each temperature. Those results were compared with the results predicted by the random pore model whose formulation does not depend on the varied structural parameters. This comparison denounced that the random pore model is only appropriate for certain washcoat structures. A maximum deviation (underprediction) of the random pore model was found to be about 37 – 74% in the temperature range 300–623 K.

The multi-scale reaction–diffusion model results of CO oxidation were compared with the performance of the 1D pseudo-homogeneous reaction–diffusion model, taking into account effective transport coefficients calculated with the random pore model and with the multi-scale diffusion model. Good agreement between both reaction–diffusion models was observed by considering the later fashion to obtain the effective transport properties for the 1D model. Based on such findings, the present study suggests a methodology to include in a full-scale reactor model the internal diffusion limitations by coupling such model with a 1D

washcoat model that employs pre-computed effective transport data evaluated through 3D multi-scale diffusion simulations.

Acknowledgments

This work was partially financed by the European Commission within the 7th Framework Program (260105 FC-DISTRICT).

References

Beeckman, J.W., 1991. Measurement of the effective diffusion coefficient of nitrogen monoxide through porous monolith-type ceramic catalysts. Ind. Eng. Chem. Res. 30, 428–430.

Chatterjee, A., Vlachos, D.G., 2007. An overview of spatial microscopic and accelerated kinetic Monte Carlo methods. J. Comput.-Aided Mater. Des. 14, 253–308.

dos Santos, L.O.E., Philippi, P.C., Fernandes, C.P., de Gaspari, H.C., 2002. Three-dimensional reconstruction of porous microstructures with the superposed spheres method. In: Proceedings of the ENCIT 2002, Caxambu - MG, Brazil, CIT02-0449.

Fechete, I., Wang, Y., Védrine, J.C., 2012. The past, present and future of heterogeneous catalysis. Catal. Today 189, 2–27.

Hayes, R.E., Kolaczkowski, S.T., Li, P.K.C., Awdry, S., 2000. Evaluating the effective diffusivity of methane in the washcoat of a honeycomb monolith. Appl. Catal., B 25, 93–104.

Hayes, R.E., Liu, B., Moxom, R., Votsmeier, M., 2004. The effect of washcoat geometry on mass transfer in monolith reactors. Chem. Eng. Sci. 59, 3169–3181.

Holladay, J.D., Hu, J., King, D.L., Wang, Y., 2009. An overview of hydrogen production technologies. Catal. Today 139, 244–260.

Irani, M., Alizadehdakhel, A., Pour, A., Hoseini, N., Adinehnia, M., 2011. CFD modeling of hydrogen production using steam reforming of methane in monolith reactors: surface or volume-base reaction model?. Int. J. Hydrogen Energy 36, 15602–15610.

Kee, R.J., Grcar, J.F., Smooke, M.D., Miller, J.A., 1985. Premix: A Fortran Program for Modeling Steady Laminar One-Dimensional Premixed Flames. Technical Report SAND85-8240, Sandia National Laboratories.

Keil, F.J., 1999. Diffusion and reaction in porous networks. Catal. Today 53, 245–258.

Kolaczkowski, S.T., Chao, R., Awdry, S., Smith, A., 2007. Application of a CFD code (Fluent) to formulate models of catalytic gas phase reactions in porous catalyst pellets. Chem. Eng. Res. Des. 85, 1539–1552.

Kočí, P., Štěpánek, F., Kubíček, M., Marek, M., 2006. Meso-scale modelling of CO oxidation in digitally reconstructed porous Pt/γ-Al_2O_3 catalyst. Chem. Eng. Sci. 61, 3240–3249.

Kočí, P., Novák, V., Štěpánek, F., Marek, M., Kubíček, M., 2010. Multi-scale modelling of reaction and transport in porous catalysts. Chem. Eng. Sci. 65, 412–419.

Mladenov, N., Koop, J., Tischer, S., Deutschmann, O., 2010. Modeling of transport and chemistry in channel flows of automotive catalytic converters. Chem. Eng. Sci. 65, 812–826.

More, H., Hayes, R.E., Liu, B., Votsmeier, M., Checkel, M.D., 2006. The effect of catalytic washcoat geometry on light-off in monolith reactors. Top. Catal. 37, 155–159.

Novák, V., Štěpánek, F., Kočí, P., Marek, M., Kubíček, M., 2010. Evaluation of local pore sizes and transport properties in porous catalysts. Chem. Eng. Sci. 65, 2352–2360.

Novák, V., Kočí, P., Štěpánek, F., Marek, M., 2011. Integrated multiscale methodology for virtual prototyping of porous catalysts. Ind. Eng. Chem. Res. 50, 12904–12914.

Novák, V., Kočí, P., Marek, M., Štěpánek, F., Blanco-García, P., Jones, G., 2012. Multi-scale modelling and measurements of diffusion through porous catalytic coatings: an application to exhaust gas oxidation. Catal. Today 188, 62–69.

Poling, B.E., Prausnitz, J.M., O'Connel, J.P., 2001. The Properties of Gases and Liquids. McGraw-Hill; New York.

Ramanathan, K., West, D.H., Balakotaiah, V., 2004. Optimal design of catalytic converters for minimizing cold-start emissions. Catal. Today 98, 357–373.

Salciccioli, M., Stamatakis, M., Caratzoulas, S., Vlachos, D.G., 2011. A review of multiscale modeling of metal-catalyzed reactions: mechanism development for complexity and emergent behavior. Chem. Eng. Sci. 66, 4319–4355.

Salejova, G., Grof, Z., Solcova, O., Schneider, P., Kosek, J., 2011. Strategy for predicting effective transport properties of complex porous structures. Comput. Chem. Eng. 35, 200–211.

Sharma, R.K., Cresswell, D.L., Newson, E.J., 1991. Effective diffusion coefficients and tortuosity factors for commercial catalysts. Ind. Eng. Chem. Res. 30, 1428–1433.

Satterfield, C.N., 1970. Mass Transfer in Heterogeneous Catalysis. MIT Press, Cambridge, MA.

Stutz, M.J., Poulikakos, D., 2008. Optimum washcoat thickness of a monolith reactor for syngas production by partial oxidation of methane. Chem. Eng. Sci. 63, 1761–1770.

Twigg, M.V., 2011. Catalytic control of emissions from cars. Catal. Today 163, 33–41.

Vlachos, D.G., Caratzoulas, S., 2010. The roles of catalysis and reaction engineering in overcoming the energy and the environment crisis. Chem. Eng. Sci. 65, 18–29.

Vlachos, D.G., Mhadeshwar, A.B., Kaisare, N.S., 2006. Hierarchical multiscale model-based design of experiments, catalysts, and reactors for fuel processing. Comput. Chem. Eng. 30, 1712–1724.

Voltz, S.E., Morgan, C.R., Liederman, D., Jacob, S.M., 1973. Kinetic study of carbon monoxide and propylene oxidation on platinum catalysts. Ind. Eng. Chem. Prod. Res. Dev. 12, 294–301.

Wakao, N., Smith, J.M., 1962. Diffusion in catalyst pellets. Chem. Eng. Sci. 17, 825–834.

Wheeler, A., 1955. Catalysis, vol. 2. Reinhold, New York, pp. 105–165 (Chapter 2).

Wood, J., Gladden, L.F., 2002. Modelling diffusion and reaction accompanied by capillary condensation using three-dimensional pore networks. Part 1. Fickian diffusion and pseudo-first-order reaction kinetics. Chem. Eng. Sci. 57, 3033–3045.